2 Density Functional Theory and Applications to Transition Metal Oxides

David J. Singh

Oak Ridge National Laboratory

Oak Ridge, TN 37831-6056, USA

Contents

1 Introduction

These are the lecture notes for a talk in a Course on Correlated Electrons: From Models to Materials held in Juelich in September, 2012. This lecture is intended to provide an introductory description of standard density functional calculations, with emphasis on oxides. In the context of the course it is a starting point for the advanced correlated methods that will be discussed in the following lectures.

This chapter consists of two main parts. The first part is a very basic introduction to density functional theory (DFT). The second part focuses on a particular aspect of transition metal oxide physics, that is magnetism and the formation of magnetic moments illustrated by the example of three rather different perovskite compounds, $SrMnO_3$, $SrTcO_3$ and $SrRuO_3$.

2 Density functional theory in condensed matter physics

It is fair to say that DFT calculations play a central role in condensed matter theory and have revolutionized the way we understand the physical properties of solids today. This chapter discusses aspects of DFT in relation to correlated materials and its use in providing microscopic understanding in diverse systems.

DFT, and the widely used local density approximation (LDA) to it, were formulated in the 1960's in two seminal papers by Kohn, Hohenberg and Sham [1, 2] and started to be applied to real solids in the 1970's. Normally, when one uses approximations, one imagines that the availability of better computers would mean that one could do better and use more exact theories. Computer speeds have followed Moore's law from that time to the present, increasing by approximately three orders of magnitude per decade, or by $\sim 10^9$ from the ~ 10 MFlop computers of the late 1970's to the present state of the art of ~ 10 PFlops as realized on the Fujitsu K computer in 2011.

10^9 is a big number. A person with a dollar (or Euro) standing outside a McDonald's can eat at the most famous restaurant in the world. A billionaire has more options, and one should take note if he chooses the dine at the same place. Today, DFT calculations based on the LDA and the computationally similar generalized gradient approximations (GGAs) remain the standard workhorse in condensed matter. This can perhaps be appreciated by noting some citation statistics. As of this writing, the paper of Perdew, Burke and Ernzerhof [3], which lays out one of the more commonly used generalized gradient approximations for solids has been cited 21,557 times, including 4,056 times in 2011 alone, while that of Perdew and co-workers laying out the so-called "PW91" functional [4], which is another common functional was cited 9,084 times, including 845 times in 2011. This reflects just how useful these approximations are.

There are many reasons for the popularity and successes of DFT calculations. Two particularly important ones are (1) the fact DFT calculations are based on the chemical compositions and structures of materials without the use of intervening models and (2) the fact that such calculations, while approximate, are predictive.

Condensed matter physics increasingly focuses on materials that are structurally and chemically complex. This trend started with the 1986 discovery of cuprate superconductivity in $(La,Ba)_2CuO_4$, which is a layered perovskite material. This was closely followed by discoveries in increasingly complex materials, $YBa_2Cu_3O_{7-\delta}$, $Bi_2SrCu_2O_8$, and $HgBa_2Ca_2Cu_3O_{8+\delta}$. Approximate DFT calculations were helpful in establishing the large scale features of the electronic structure of these cuprates [5, 6]. In complex materials it is particularly difficult to sort out the key structural features and how they relate to the physical properties. One may guess the shape of the Fermi surface of Na metal without recourse to detailed calculations but it is unlikely that one would correctly guess the complex multisheet Fermi surfaces of materials like $YBa_2Cu_3O_7$. A more recent example comes from the iron-pnictide superconductors, where DFT calculations revealed a very non-oxide-like electronic structure and the presence of relatively small disconnected multisheet Fermi surfaces that are of importance for understanding the superconductivity [7, 8].

There have been many excellent reviews of DFT and DFT calculations, and so we do not attempt to provide another one here. We simply mention a few relevant points and refer the reader to the extensive literature on this subject for detailed discussions. Some excellent resources are the books, *Density Functional Theory of Atoms and Molecules*, by Parr and Yang [9], *Density Functional Methods in Physics*, by Dreizler and da Provincia [10], *Density Functionals: Where do the come from, why do they work?*, by Ernzerhof, Burke and Perdew [11], *Theory of the Inhomogeneous Electron Gas*, by Lundqvist and March [12], and the review article by Callaway and March [13].

Finally, we note that while DFT is an exact theory, practical applications require tractable approximations to the DFT functional. The success of DFT really rests on the fact that relatively simple and general approximate forms such as the LDA and GGAs yield very good descriptions of the properties of diverse solid state and molecular systems. The remarkable success of simple approximations, such as the local density approximation, in accurately describing the properties of condensed matter was hardly anticipated before detailed calculations were performed starting in the 1970's. There has been theoretical discussion of the reasons for the successes of simple approximations like the LDA since then. However, it remains the case that approximate DFT calculations are used to predict many properties of materials based mainly on the fact that previous calculations have shown these properties to be in good agreement with experiment on other materials. Put another way, the local density approximation is built around the many body physics of the uniform electron gas. Nonetheless it is able to describe materials that have highly inhomogeneous electron distributions that at first sight have nothing to do with the electron gas. The success of these simple approximations in describing diverse properties of materials without experimental input provides an explanation for the conundrum, posed above, i.e. the long lived popularity of DFT methods.

A simple example is bcc Fe, which is a commonly known ferromagnet. Like Fe, the uniform electron gas shows magnetism. However, the magnetism of the uniform electron gas only occurs at densities of $\sim 10^{20}$ cm^{-3} and below [14]. In contrast the average electron density of bcc Fe is 2.2×10^{24} cm^{-3} including all electrons and 6.8×10^{23} cm^{-3} if only the valence electrons are

included. Thus Fe shows ferromagnetism at densities four orders of magnitude above where the uniform electron gas does. So the non-uniform electron gas constituting Fe has very different properties than the uniform electron gas. Nonetheless, this non-uniform electron gas is extremely well described by the local density approximation, with a moment that agrees within ∼3% of the experimental value, and a lattice parameter also in good agreement.

The point is that even though the LDA and GGAs are seemingly rather simple approximations they have certain advantages. These are (1) that they are truly ab-initio, in the sense of not requiring any input from experiment specific to the material being studied – this is key to making predictions – and (2) they are often rather precise for properties of materials, including non-trivial but important properties such as Fermi surfaces. In fact, the predictions made by simple LDA and GGA calculations have been transformational in many areas of condensed matter, e.g. the prediction of high pressure phases and their properties, complex Fermi surfaces of materials such as the high T_c cuprate superconductors, and many other areas.

Clearly, as will be shown in subsequent lectures of this school, these simple approximations have important deficiencies, especially in treating so-called strongly correlated systems. The simplest example is the failure of these approximations to describe the insulating ground states of Mott insulators, such NiO and the physics associated with the electron correlations that produce such ground states. In devising needed improvements to these approximations for treating correlated materials it is perhaps helpful to keep in mind the features of the LDA that make it so successful – absence of empirical or material specific parameters or tunable heuristics (i.e. making choices based on knowledge of the material in question) and its ability to make predictions based on the chemical composition and structure of a material and not much else.

2.1   Basics

Density functional theory itself is, as the name implies, an exact theorem. It states that the ground state energy, E of an interacting system subject to an external potential, $V_{ext}(\mathbf{r})$ is a functional of the density, $E=E[\rho(\mathbf{r})]$, and furthermore that the actual density, $\rho(\mathbf{r})$ is the density that minimizes this total energy functional. This means that the density $\rho(\mathbf{r})$, which is a non-negative function of the three spatial variables, can be used as the fundamental variable in quantum mechanical descriptions of the correlated system, as opposed to the many-body wavefunction, which is a function of $3N$ spatial variables for an N particle system.

As mentioned, while DFT is an exact theorem, the important aspect is that there are practical approximations based on it that can be applied to a wide variety of materials with frequently useful results. The first practical approximation to DFT was the local density approximation (LDA), which was proposed by Kohn and Sham in the paper where they derived the so-called Kohn-Sham equations [2]. They proceeded by observing that any density corresponding to an interacting N electron density can be written as the density corresponding to some N electron non-interacting wavefunction. Thus,

$$\rho(\mathbf{r}) = \sum_i \varphi_i^*(\mathbf{r})\varphi_i(\mathbf{r}); i = 1, 2, ..., N, \tag{1}$$

where the φ_i are the so-called Kohn-Sham orbitals and are orthonormalized functions. While the density can be exactly written in this way, it is to be emphasized that a determinant of the Kohn-Sham orbitals would typically be a very poor approximation to the true wavefunction, and so in general the Kohn-Sham orbitals are quite distinct from the actual wavefunction of a system.

Kohn and Sham then separated from the functional, $E[\rho]$, some large terms that are readily evaluated, leaving a presumably smaller remainder $E_{xc}[\rho]$ to be approximated.

$$E[\rho] = T_s[\rho] + E_{ext}[\rho] + U_{Hartree}[\rho] + E_{xc}[\rho], \tag{2}$$

where E_{ext} is the interaction with the external potential, $U_{Hartree}$ is the Hartree energy,

$$U_{Hartree}[\rho] = \frac{e^2}{2} \int \mathrm{d}^3\mathbf{r}\mathrm{d}^3\mathbf{r}' \ \frac{\rho(\mathbf{r})\rho(\mathbf{r}')}{|\mathbf{r} - \mathbf{r}'|}. \tag{3}$$

and T_s is the non-interacting kinetic energy of the Kohn-Sham orbitals (which is not the true kinetic energy of the many-body system).

The Kohn-Sham equations can then be derived using the fact that the true density is the density that minimizes $E[\rho]$,

$$\left(T_s + V_{ext} + V_{Hartree} + V_{xc}\right)\varphi_i = \varepsilon_i\varphi_i, \tag{4}$$

where the ε_i are the Kohn-Sham eigenvalues, which are not equal to true excitation energies of the system, T_s is the single particle kinetic energy operator and the various potential terms V are functional derivatives of the corresponding energy terms with respect to $\rho(\mathbf{r})$.

The local density approximation is obtained by writing,

$$E_{xc}[\rho] = \int \mathrm{d}^3\mathbf{r} \ \rho(\mathbf{r})\epsilon_{xc}(\rho(\mathbf{r})), \tag{5}$$

where $\epsilon_{xc}(\rho)$ is approximated by a local function of the density, usually that which reproduces the known energy of the uniform electron gas.

To treat spin-polarized systems, a generalization to so-called spin-density functional theory is needed to produce useful approximations. The generalization is straight-forward. For a collinear magnetic system one replaces ρ by the two spin-densities, $\rho^\uparrow$ and $\rho^\downarrow$, so that the energy becomes a functional of these two spin-densities, $E[\rho^\uparrow, \rho^\downarrow]$, $E_{xc}[\rho^\uparrow, \rho^\downarrow]$, and $V_{xc}[\rho^\uparrow, \rho^\downarrow]$ [15]. Replacing E_{xc} by the exchange-correlation energy of the partially spin polarized electron gas using the local spin densities yields the so-called local spin density approximation (LSDA), which is a very popular and effective method at least as a starting point. In the more general non-collinear case, the magnetization has both a magnitude and direction that vary with position, and so the density takes four components, instead of two as in the collinear case. In this case, the LSDA is formulated in terms of 2x2 density and potential matrices, $\boldsymbol{\rho}$ and $\mathbf{V}$, which can be expanded in terms of Pauli spin matrices, e.g. $\boldsymbol{\rho} = \rho\mathbf{1} + \mathbf{m} \cdot \boldsymbol{\sigma}$ [15]. This formalism, with a local approximation in which the exchange correlation term is again taken from the uniform electron gas with the same local polarization magnitude and a direction for $\mathbf{V}_{xc}$ parallel to the

local magnetization direction, yields a useful non-collinear version of the LSDA that has been widely applied to non-collinear systems [16].

The generalized gradient approximations (GGAs) are the other commonly used class of density functionals in solids. They use the local gradient as well as the density in order to incorporate more information about the electron gas in question, i.e. $\epsilon_{xc}(\rho)$ is replaced by $\epsilon_{xc}(\rho, |\nabla\rho|)$. These generalized gradient approximations, which originated in the work of Langreth and Mehl [17] and Perdew and co-workers [4] are very different from gradient expansions, which lead to greatly degraded results from the LDA.

Actually, considering how different the electron gas in solids is from the uniform electron gas, it is perhaps not surprising that a Taylor expansion, which treats solids as a minor perturbation of the homogeneous gas, would not work. The modern GGA's are instead rather sophisticated functionals build around sum rules and scaling relations for the exchange-correlation hole in the general non-uniform electron gas.

The central relation is the adiabatic connection formula, which in Rydberg units is

$$E_{xc}[n] = \int d^3\mathbf{r} \int d^3\mathbf{r}' \frac{n(\mathbf{r})n(\mathbf{r}')}{|\mathbf{r} - \mathbf{r}'|}(\bar{g}[n, \mathbf{r}, \mathbf{r}'] - 1) = \int d^3\mathbf{r} \int d^3\mathbf{r}' \frac{n(\mathbf{r})\bar{n}_{xc}(\mathbf{r}, \mathbf{r}')}{|\mathbf{r} - \mathbf{r}'|}, \quad (6)$$

where $\bar{g}$ is the coupling-constant average (from the non-interacting $e^2 = 0$ value to the physical value of e^2) of the pair distribution function, n is the density as usual and $\bar{n}_{xc}$ is defined by the equation. This may be understood as the interaction energy of each electron with its exchange correlation hole less the energy needed to "dig out" the hole. The latter includes contributions to the kinetic energy beyond the single-particle level. The LDA then consists of the replacement of $n(\mathbf{r}')\bar{g}[n, \mathbf{r}, \mathbf{r}']$ by $n(\mathbf{r})\bar{g}^h(n(\mathbf{r}), |\mathbf{r} - \mathbf{r}'|)$, where $\bar{g}^h$ is the coupling constant averaged pair distribution function of the homogeneous electron gas.

Modern GGA functionals are built using the adiabatic connection formula based on knowledge of exact sum rules, scaling relations and limits for the exchange correlation hole in the general non-uniform case. The simplest such sum rule is that the exchange correlation hole contains a charge of exactly unity. This rule, which is satisfied by the LDA, and the spherical Coulombic average in Eqn. 6 have been used to explain why such a simple approximation works as well as it does (see especially, Ref. [12] for clear discussions of this).

2.2 DFT, Jellium and Hartree-Fock

In thinking about DFT and approximations, it is helpful to remember what it is not, particularly when considering what one might do to improve such approximations to DFT. Sometimes it is said that LDA or GGA calculations represent either a jellium or a Hartree-Fock approximation to the many-body system. One purpose of this section is to emphasize that this is not really correct.

Hartree-Fock, unlike approximate DFT methods, is a variational method based on the exact Hamiltonian. The Hartree-Fock energy is always higher than the true energy. Hartree-Fock consists of restricting the wavefunctions to Slater determinants. This gives an exact exchange

description with no correlation. Hartree-Fock generally overestimates the band gaps of semi-conductors and insulators, opposite to standard approximate DFT methods, such as the LDA. Furthermore, importantly, unlike DFT, Hartree-Fock cannot describe metals, since all metals are unstable in this approximation. Thus it is incorrect to consider a starting description of a metal within e.g. the LSDA as representing a Hartree-Fock description to which one may add correlations as if none were present in this starting point. Also, it should be noted that approximate DFT because of its uncontrolled approximations is not self-interaction free. Specifically, while the exact exchange correlation hole has a charge of exactly unity, this is not the case for e.g. the LDA in a non-uniform electron gas. Hartree-Fock on the other hand has an exchange hole that does contain a charge of exactly unity and therefore is self-interaction free.

The distinction between Hartree Fock and approximate DFT is also important from a historical point of view. Several approximations similar to the LSDA had been proposed and widely used prior to the development of Kohn-Sham DFT. The $X\alpha$ method of Slater and co-workers is the most widely known such method [18]. However, while the formalism of the $X\alpha$ method is very similar in appearance to that of the LSDA, from a conceptual point of view it is very different. In particular, the $X\alpha$ method was viewed as a simplification of the Hartree-Fock method, i.e. an approach for fast approximate Hartree-Fock calculations. As such, it was typically parametrized to reproduce Hartree-Fock as well as possible, often taking the band gap as a quantity that should be fit. When used in this way it gave many interesting and useful results, e.g. the body of work produced by J.C. Slater and his group, but did not approach the predictive capabilities of modern approximate DFT methods. The key point is that approximate DFT methods, like the modern LDA, are approximations to an exact theory that has density and energy as fundamental quantities, and which does not reproduce band gaps. This new view led to the use of the energy of the uniform electron gas in the LDA, rather than a functional form that comes from the high density exchange, and is what underlies the much better predictive power of the modern approximate DFT methods.

We now turn to jellium. Jellium is the uniform electron gas that forms the basis of the LDA. It is a metal that at densities appropriate to solids is far from magnetism. It is also a gas and as such has no shear strength. In solid state physics, perhaps the simple materials closest to jellium are the alkali metals, e.g. K or Cs, which are indeed very soft metals that are far from magnetism. Also, like jellium, they have nearly spherical Fermi surfaces. In any case, the implication of regarding the LDA as a jellium model is that one adopts a view in which solids that are well described by the LDA are essentially well described as a uniform electron gas with weak perturbation by pseudopotentials representing the atomic cores. However, while LDA and GGA calculations do provide a reasonable description of K and Cs, they provide an equally good description of materials like diamond and Al_2O_3, which are insulators and not only support shear modes, but in fact are among the stiffest known materials.

The point is that solids are not like blueberry muffins (a kind of small cake with embedded berries that is popular in the United States). The characteristic of blueberry muffins is that they taste roughly the same independent of the exact number or distribution of the blueberries inside them. Solids are not at all like that. Instead they show a tremendous diversity of properties

YBa$_2$Cu$_3$O$_7$ YNi$_2$B$_2$C   LaFeAsO
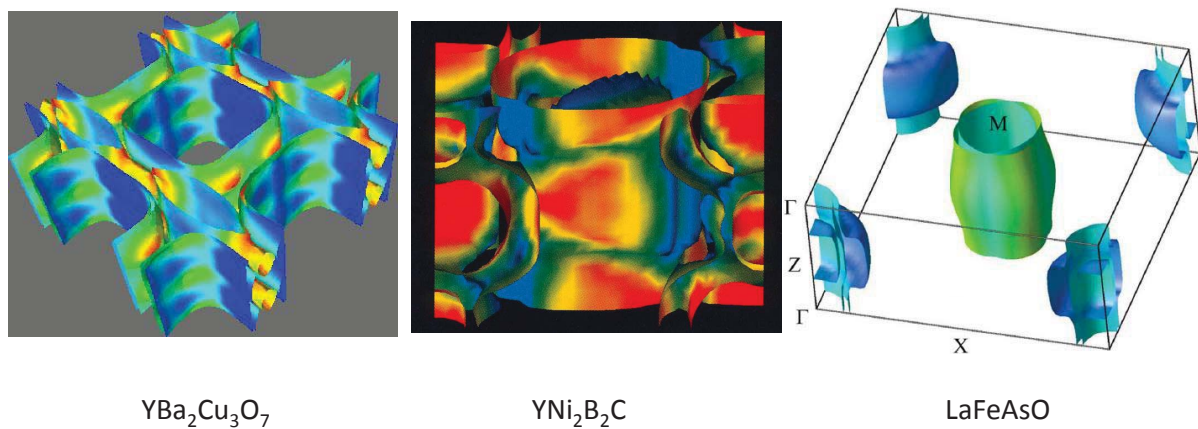
Fig. 1: *The Fermi surfaces of three superconductors, YBa$_2$Cu$_3$O$_7$ (left, following Ref. [6]), YNi$_2$B$_2$C (middle, following Ref. [19]) and LaFeAsO (right, following Ref. [7]).*

depending on the exact type and arrangement of the atoms making them up. Many of the diverse observed behaviors of materials are in fact rather well described by approximate DFT calculations. The fact that the properties of Cs appear to be like those of jellium, while those of diamond appear to be very different does not imply that diamond is a more strongly correlated material than Cs but is simply a reflection of the fact that the properties of non-uniform electron gasses, are different from those of the uniform electron gas. This emphasizes the fact that LDA and GGA approximations do not represent some kind of slowly varying approximation for the electron gas and so they are often well able to describe the highly non-uniform electron gasses that comprise condensed matter.

Related to this, in solid state physics it is very useful to start with simple models in order to understand phenomena. For metals, jellium is a very useful pedagogical starting point, and because of this many common formulas for metals are written in text books for the case of a spherical Fermi surface. On the other hand the Fermi surfaces of real metals are often very complex, as shown for three superconductors in Fig. 1.

All three of these superconductors show multiple sheets, with no obvious relationship to a simple sphere. However, these Fermi surfaces from LDA calculations agree remarkably well with experiment. This was perhaps particularly surprising in the case of the high T_c cuprate, YBa$_2$Cu$_3$O$_7$, since like the other cuprates it is in close proximity to undoped phases (YBa$_2$Cu$_3$O$_6$ in this case) that are Mott insulators and are not even qualitatively described by standard LSDA calculations.

In any case, the Fermi surface plays the central role in setting the low energy properties of a metal. Also, superconductivity is fundamentally an instability of the Fermi surface, and so knowledge of the Fermi surface can reveal a lot about the nature of the superconductivity in a given compound. For example, all three materials shown in Fig. 1 have crystal structures that may be described as layered. However, as shown, the Fermi surfaces of the boro-carbides and boro-nitrides (LuNi$_2$B$_2$C, YNi$_2$B$_2$C, etc.) are clearly three dimensional and in particular do not

take the form of cylinders. This was one of the first indications following their discovery that the superconductivity of these materials is unrelated to that of the high T_c cuprates [20]. It is also an illustration of why approximate DFT has become so widely used – DFT calculations predicted the three dimensionality of the Fermi surfaces and some other important aspects well in advance of experimental measurements.

Returning to the jellium model, in characterizing the nature of correlations in a material, the fact that experiment may show that a certain metal cannot be described by spherical Fermi surface formulas, does not in itself mean that it cannot be described by detailed DFT calculations, nor does it in itself imply that a material is strongly correlated (although it may be). In other words, unconventional behavior in relation to simple jellium based models could be a consequence of strong correlations, or it could alternatively be a consequence of a non-trivial electronic structure that is, however, still well described by approximate DFT calculations. It is important to sort this out in each case. Also, there is sometimes confusion that arises from the simplifications in spherical Fermi surface models. For example, in a metal the bands and their dispersions at the Fermi energy E_F play a central role in the low energy physics.

The band velocity, $\mathbf{v_k} = \nabla_\mathbf{k} \varepsilon(\mathbf{k})$, where $\varepsilon(\mathbf{k})$ are the band energies, is an important quantity both for transport and thermodynamic properties. Within Boltzmann theory the conductivity is essentially related to the velocity, $\sigma_{xx} \sim N(E_F)\langle v_x^2 \rangle \tau$, where τ is an inverse scattering rate, $\langle\ \rangle$ denotes the Fermi surface average, and $N(E_F)$ is the density of states at E_F. The square of the Drude plasma frequency, which can be measured from infrared optics, is given by a similar factor, $N(E_F)\langle v_x^2 \rangle$. However, for a parabolic band (spherical Fermi surface) system this can also be written as n/m, where m is the effective mass, and n is the carrier density (volume of the Fermi surface), and similarly one can also eliminate n in favor of the Fermi energy, E_F relative to the band edge. However, it is to be emphasized that infrared optics does not measure E_F nor does it measure n or m (and obviously considering the excitation energy it cannot be sensitive to such high energy properties), but only a certain integral over the actual Fermi surface.

The bottom line is that extraction of high energy quantities such as Fermi energy and band filling from experiments such as transport, infrared optics, superconducting properties etc., is generally model dependent and simple conclusions about high energy properties based on such measurements should be carefully considered. One exception is the extraction of the Fermi surface volume in layered materials from Hall data, which has been shown to be exact, independent of the detailed band dispersions and Fermi surface shape provided that the Fermi surfaces are all open (e.g. cylinders) in the third dimension [21].

3   Aspects of magnetism in oxides

In this section we illustrate some aspects of magnetism in oxides using three compounds, cubic perovskite $SrMnO_3$, perovskite $SrTcO_3$ and the ferromagnetic perovskite metal $SrRuO_3$.
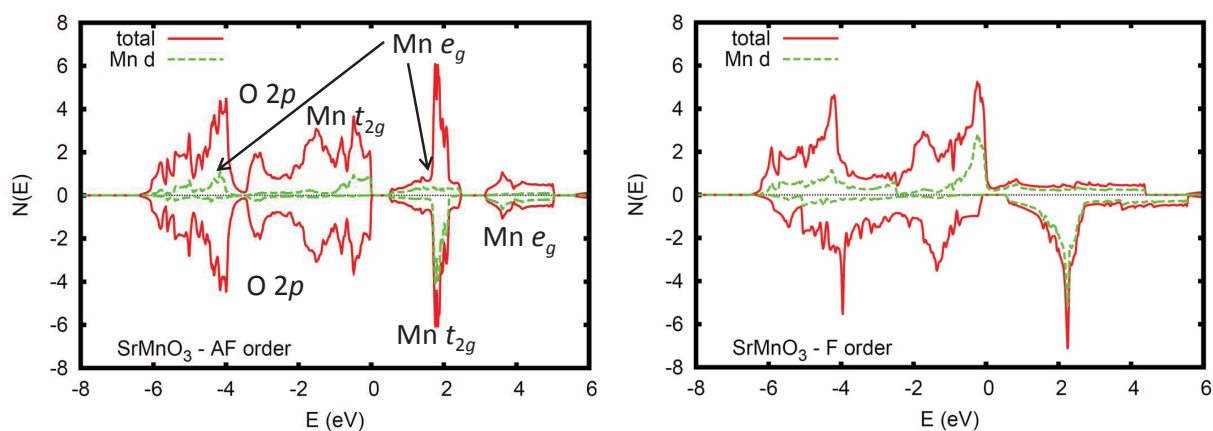
3.1   SrMnO$_3$

Manganites attracted much attention because of the colossal magnetoresistance effect (CMR) and novel exchange couplings in materials like (La,Ca)MnO$_3$ and (La,Sr)MnO$_3$. starting in the 1950's [22–25] and then again following the rediscovery and enhancement of the CMR effect the 1990's [26, 27]. The basic features of the electronic structure from point of view of band theory have been extensively elucidated by many authors. (see e.g. [28]). Here we focus on the end-point compound SrMnO$_3$.

SrMnO$_3$ has both hexagonal and cubic polytypes, with hexagonal being the ground state. Here we consider the cubic polytype, which is an antiferromagnet with Neel temperature, T_N=240 K [29]. The related, and more studied compound, CaMnO$_3$ has an orthorhombic structure, characterized by tilts of the MnO$_6$ octahedra, up to $T_s \sim 720$ K, above which it takes a different rhombohedral structure. The ground state is a G-type antiferromagnet (nearest neighbor antiferromagnetism) with a Neel temperature T_N=124 K. Importantly, the resistivity is insulating both above and below T_N, which is a characteristic of a correlated (i.e. Mott type) insulator [30, 31]. Interestingly, there is a metal-insulator transition at the structural transition, T_s, and in the rhombohedral phase CaMnO$_3$ is metallic.

Standard DFT calculations for CaMnO$_3$ predict a G-type antiferromagnetic insulator with a small band gap [28]. Like CaMnO$_3$, standard DFT calculations (without U) yield a small band gap insulator for SrMnO$_3$ (see Fig. 2) with G-type AFM order. In contrast, if ferromagnetic order is imposed, SrMnO$_3$ is predicted to be a metal. Here we discuss some calculations, which were done with the LAPW method using the standard PBE GGA functional at the experimental cubic lattice parameter (a=3.808 Å), and are basically the same as previously reported results. Integration of the spin density within the Mn LAPW spheres, radius 1.9 Bohr, yields moments within the spheres of 2.52 μ_B for the ferromagnetic (corresponding to 3 μ_B per formula unit for the whole cell), and a similar value of 2.41 μ_B for the ground state antiferromagnetic structure. This weak dependence of the moment on the ordering means that even at the level of standard band calculations, SrMnO$_3$ behaves like a local moment magnet.

From an experimental point of view SrMnO$_3$ is a borderline material. It is clearly insulating both above and below T_N, although very small perturbations make it metallic [30]. In any case, it illustrates some important features of the band description of correlated oxides.

First of all, there can be some ambiguity, because band calculations can yield an insulating state and so it can in some cases be difficult to decide if a material is a band insulator or a true Mott-Hubbard system. In a Mott system, one expects insulating behavior independent of magnetic order, one manifestation is that the resistivity shows similar insulating behavior both above and below T_N. In contrast the band picture in a material like SrMnO$_3$ implies that the conductivity should increase when the AFM order is destroyed above T_N since it relates to the specific magnetic order. Also, in strongly correlated transition metal oxides, the gaps predicted by standard DFT calculations are often very small in comparison with experiment, for example tenths of an eV in materials that have several eV band gaps, such as NiO. Essentially, while there can be a band gap for such materials in standard band calculations, the description of the

Fig. 2: *Electronic density of states of cubic perovskite SrMnO$_3$ as obtained with the PBE GGA. The calculations were done using the LAPW method and the projections are onto the Mn LAPW spheres of radius 1.9 Bohr. Majority spin is shown above the horizontal axis, and minority below. The left panel shows the result for the G-type antiferromagnetic ground state, while the right panel is for ferromagnetic order.*

electronic structure and the true nature of the gap is qualitatively incorrect. Cases like SrMnO$_3$ are less clear. This is because there is not a clear experiment showing the magnitude of the gap in the paramagnetic phase for this material, and because very tiny dopings produce metallic conduction about T_N suggesting that the material is almost metallic [30]. In general, care is needed in deciding the extent and nature of correlations in materials.

The second point is the connection between structure and correlations. CaMnO$_3$ is a much more clear case of a Mott insulator that SrMnO$_3$, which from an experimental point of view is more borderline. The principal difference between the two materials is structural, i.e. that in CaMnO$_3$ the MnO$_6$ octahedra are rotated yielding an orthorhombic structure. Such a structural distortion will generally narrow the bands (especially the e_g band) in a perovskite, favoring a correlated state. The Mott transition is typically first order and is frequently strongly coupled to structure. Thus properties of a metal near a Mott transition, as in the cuprate superconductors, can be very different from those of the nearby Mott insulator. The presence of the Mott phase in materials like cuprates shows the importance of the interactions that give rise to it on both sides of the metal-insulator transition, but the manifestation of these interactions in the physical properties can be very different in these different phases. An interesting note is that, even though standard band calculations yield completely wrong descriptions of the Mott phases, many aspects of the nearby conducting phases, such as the Fermi surfaces of YBa$_2$Cu$_3$O$_7$, can be well described. While, as will be discussed in other chapters in this volume, there has been significant recent progress, it remains challenging to add the essential effect of the missing correlations to DFT calculations, without destroying the good features of those calculations, or changing from a first principles approach to an approach based on model parameters.
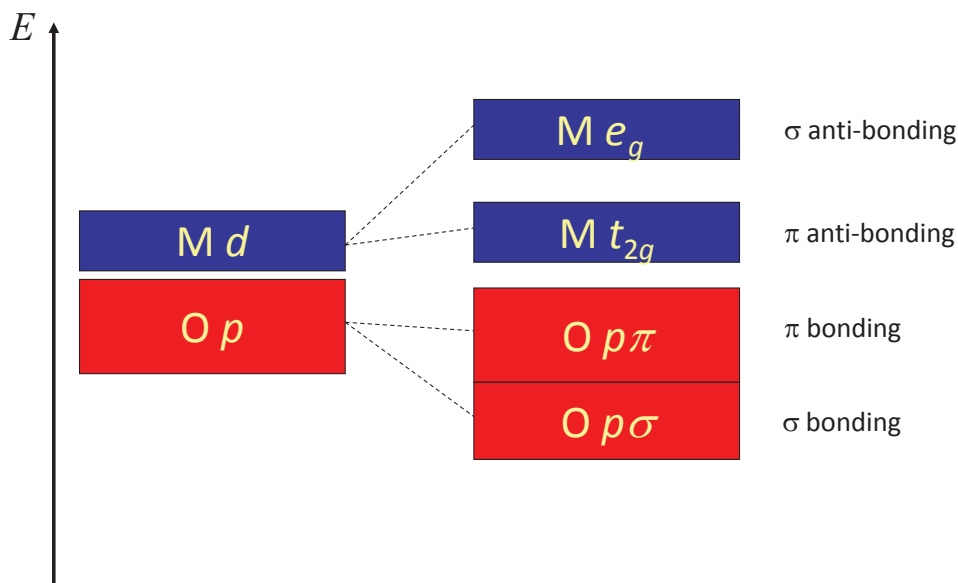
Fig. 3: *The octahedral crystal field splitting in transition metal oxides such as SrMnO₃.*

3.2   Crystal fields, moment formation and ordering

In order to continue with our discussion of SrMnO₃, it is useful to first overview some aspects of magnetism in perovskite oxides. In the cubic perovskite ABO₃ structure the B-site ions are separated by the lattice parameter a, typically $\sim$4 Å in oxides, while the bond lengths along B-site – O – B-site paths are a/2. Thus the main interactions both for forming the electronic structure and for magnetism are through the oxygen ions, specifically the O $2p$ orbitals. These orbitals are p_x, p_y and p_z.

These orbitals mix with the transition metal d orbitals. The Pauling electronegativity of O is 3.44, which is higher than that of any transition element. Therefore the center of the transition metal d bands lies above the center of the O p bands in almost any such material (for this purpose ZnO, CdO and HgO with their full d shells are not regarded as transition metal oxides). In a cubic environment, the five d orbitals are separated by symmetry into a two-fold degenerate (per spin) e_g and a three-fold degenerate t_{2g} set.

The e_g orbitals, labeled $x^2 - y^2$ and z^2, have lobes that point towards the O ions in an octahedral environment, while the t_{2g} orbitals, xy, xz and zy point in between the O ions. If one adopts a local frame in which the p_z orbital points to the B-site ion and the p_x and p_y are oriented perpendicular to this bond, one sees that there is a strong σ bonding interaction between the p_z the e_g d orbitals on the B-site and a weaker π bonding between the O p_x, p_y orbitals and the t_{2g} d B-site orbitals. This explains the crystal field scheme in perovskites. The metal bands are formally metal d – O p antibonding combinations. The t_{2g} bands are more weakly antibonding than the e_g bands, and therefore occur lower in energy. This is shown in Fig. 3. Also it follows that in perovskites absent structure distortions, the t_{2g} bands are generally narrower than the corresponding e_g bands and also that the e_g bands have a more mixed metal d – O p character than the t_{2g} bands. Importantly, the crystal field splittings in the d bands of transition metal
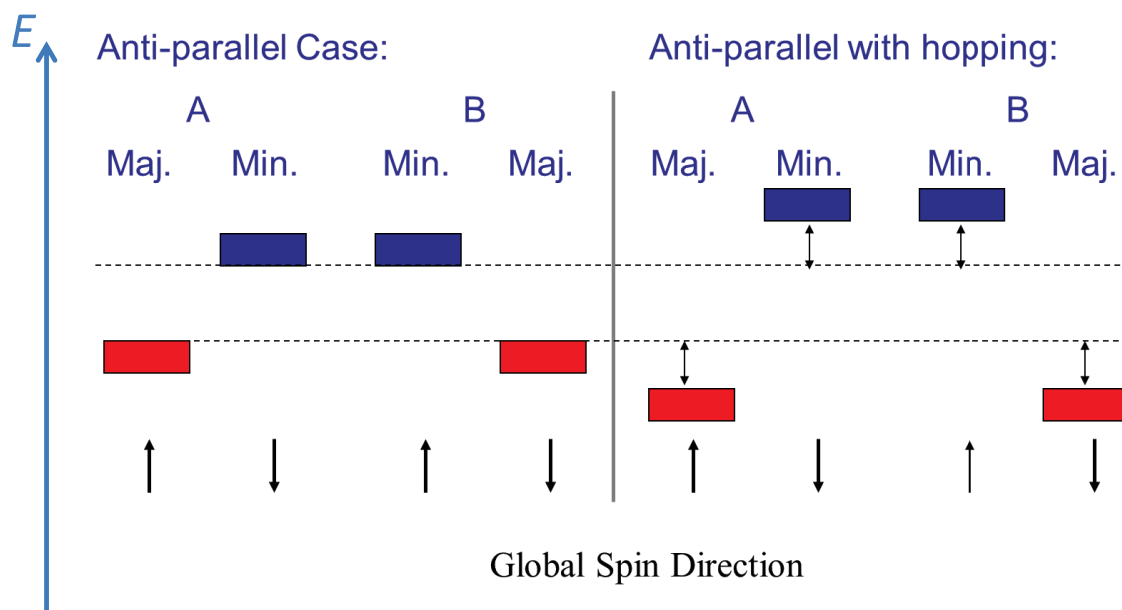
Fig. 4: *Band structure depiction of the superexchange mechanism for interaction between two transition metal ions.*

oxides are primarily due to hybridization and covalency with the p states of the neighboring O as opposed to non-spherical electrostatic potentials. As such, large crystal field splittings are an indicator of strong hybridization.

Within a local moment picture, which as mentioned is a good starting point for $SrMnO_3$, magnetism generally has two aspects: (1) Moment formation and (2) coupling of the moments at different sites to produce ordering. In most materials these two processes can be considered separately. The moment formation is driven by the on-site Hund's coupling in open shell ions, while the magnetic interactions are through the band formation, i.e. hopping between sites, which for the reasons discussed above in perovskites is expected to involve O.

For magnetic ordering, large inter-site interactions, i.e. large effective Heisenberg parameters J, or more generally large hopping integrals, should lead to high ordering temperatures. On the other hand, strong hopping implies both covalency between the B-site and O orbitals, which will reduce the on-site Hund's coupling through mixing of the orbitals and also large band width. If the band width becomes comparable to the Hund's coupling, one may expect the moments (and therefore magnetism) to be lost.

Superexchange is by far the most commonly discussed exchange mechanism in oxides. The theory for this interaction was formulated by P.W. Anderson [32] and further elucidated by Goodenough [33] and Kanamori [34]. Here we describe it within a band structure framework. The left panel of Fig. 4 shows an energy level scheme for two ions with their spins aligned antiparallel (i.e. anti-ferromagnetically, so that the majority spin is in the global spin-up direction on one site and in the opposite spin-down global direction on the other site). Allowing hopping through O mixes orbitals on different atoms within the same global spin direction. For antiparallel alignment this means that the majority spin on one atom mixes with the minority spin

on the next, and vice versa. The result is that the lower lying majority states will be pushed down in energy and the minority spin states pushed up. If the Fermi level is placed so that the majority levels are occupied, while the minority are unoccupied, the result will be a net energy lowering. On the other hand, if the spins are aligned ferromagnetically, then the majority spin on one atom mixes with the majority spin on the neighboring atom, and if this level is completely occupied there will be no gain from this and similarly for the fully unoccupied minority spin channel. Thus one has an energy gain for antiferromagnetic alignment but not for ferromagnetic. This constitutes the superexchange interaction.

So, what favors strong superexchange from a chemical point of view? Superexchange arises due to hopping between sites via O. This means that strong hopping favors strong superexchange. Cases where this can be expected are (1) transition metal atoms in high valence states such as in the cuprate superconductors (because in that case the d levels will be low in energy, i.e. close to the O $2p$ levels); (2) cases involving e_g orbitals, i.e. systems with an empty e_g in the minority spin and a full e_g in the majority spin (since e_g orbitals participate in strong σ bonds with O $2p$ orbitals); (3) straight bonds for the e_g case, since the hopping will be strongest in that case; (4) structures with short metal – O distances; and (5) heavier $4d$ and $5d$ elements to the extent that they can have moments as in $SrTcO_3$, which we discuss below (these have larger d orbitals with more covalency than $3d$ elements) [35]. With the exception of straight bonds, these are the same factors that lead to large crystal field splittings.

3.3   SrMnO$_3$ revisited

Returning to SrMnO$_3$ (Fig. 2), one has both substantial crystal field and exchange splittings of the d bands. From electron counting, there are three d electrons in Mn^{4+}, and so this should normally lead to a fully occupied majority spin t_{2g} manifold, with the other d bands empty, and a spin moment of 3 μ_B/Mn, consistent with the calculated and experimental results. The main O $2p$ bands occur in the energy range from 0 eV (top of the valence band) to $\sim$ 6 eV binding energy (-6 eV), with the $p\sigma$ in the bottom 3 eV. Focusing on the G-AFM (left panel) the minority spin shows a crystal field splitting of $\sim$ 2 eV between well defined t_{2g} and e_g manifolds. In the majority spin the occupied t_{2g} manifold overlaps the top of the O $2p$ bands due to the exchange splitting, which is a little smaller than 3 eV.

A closer examination shows Mn e_g character at the bottom of the valence bands (i.e. the bonding O $p\sigma$ - Mn e_g combination) in both spin channels but much more strongly in the majority spin. The reason for the spin dependence is that the d bands are lower in energy in the majority channel, which favors covalency through a smaller energy denominator. Thus the hybridization in SrMnO$_3$ is very spin dependent, with clearly stronger hybridization for the majority spin e_g than for the minority spin. This is important for the metallicity of the ferromagnetic ordering, and also as it is generic to perovskite manganites, it is important for the band formation of those compounds in general.
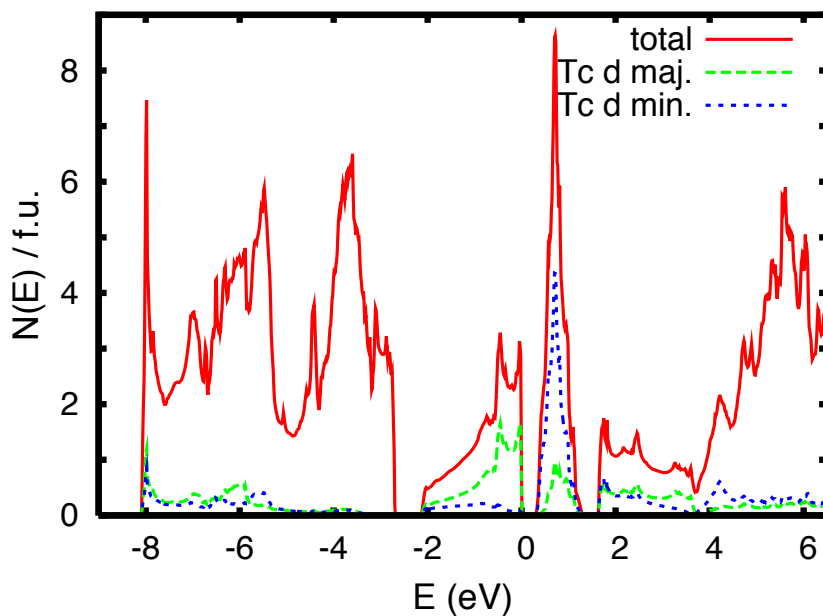
Fig. 5: *Electronic density of states of SrTcO$_3$ as obtained within the LSDA following Ref. [35]. The Tc d projections are onto the LAPW spheres of radii 2.1 Bohr.*

3.4   SrTcO$_3$

Tc is the element directly below Mn in the periodic table, i.e. it is the $4d$ analogue of the $3d$ element Mn. Tc is in general chemically similar to Mn, but as is generally the case in going from the $3d$ element to a $4d$ element, it has a lower Hund's coupling and more extended d orbitals, with the result that Tc has less tendency to form high spin compounds and has a tendency to be more covalent in compounds. Finally, Tc is larger than Mn in the sense that its Shannon ionic radii are larger than those of Mn. Structural distortions in ABO$_3$ perovskites are often understood in terms of a tolerance factor, $t = (r_A + r_O)/(\sqrt{2}(r_B + r_O))$, where r_A, r_B and r_O are the ionic radii of the A, B and O ions. Thus the tolerance factor of SrTcO$_3$ is smaller than that of SrMnO$_3$, which from a structural point of view makes it more analogous to CaMnO$_3$, and in accord with this SrTcO$_3$ forms in an orthorhombic distorted perovskite structure characterized by tilts of the TcO$_6$ octahedra.

As mentioned, the Neel temperature of CaMnO$_3$ is lower by approximately a factor of two than that of SrMnO$_3$. In contrast, SrTcO$_3$ has received recent attention because of its extremely high $T_N > 1000$ K [35]. Similar to CaMnO$_3$ and SrMnO$_3$, the ground state of SrTcO$_3$ is a G-type antiferromagnet.

The density of states for the ground state magnetic structure as obtained within the LSDA is shown in Fig. 5. As may be seen, again similar to SrMnO$_3$, a small band gap insulator is predicted. However, the electronic density of states (DOS) is qualitatively different. The projections show very strong covalency between O and Tc even for the nominal t_{2g} manifold (Tc t_{2g} – O p π antibonding combinations; recall that for SrMnO$_3$ the t_{2g} hybridization was weak and it was only the direct σ bonding e_g states that showed large hybridization). Because

of this strong covalency, the Tc d character as measured by the weight inside the 2.1 Bohr LAPW sphere amounts to only $\sim 60\%$ of the total $N(E_F)$. Furthermore, the Hund's coupling on the $4d$ Tc atoms is smaller than that on $3d$ atoms because of the more extended orbitals in this case. One can see this in the smaller exchange splitting in the Tc compound, as compared to the Mn analogue (note the exchange splitting of the t_{2g} states, ~ 1 eV).

As in $SrMnO_3$, the G-type ground state state can be understood in a simple chemical bonding picture. Hybridization occurs between states of the same global spin direction and yields the best energy lowering when occupied states mix with unoccupied states to leave bonding combinations occupied and antibonding combinations unoccupied. With G-type order, the occupied majority spin states on a given site hybridize with unoccupied minority states on each of the six neighboring sites, which is most favorable. However, unlike $SrMnO_3$, $SrTcO_3$ does not show local moment behavior at the DFT level. For example, it was found that the moments collapse to zero for ferromagnetic ordering. Rodriguez and co-workers also considered other orderings [35]. These were a so-called A-type ordering, consisting of ferromagnetic sheets of Tc stacked antiferromagnetically, a C-type arrangement with sheets of nearest neighbor antiferromagnetic Tc stacked to give ferromagnetic chains along the stacking direction, and a G-type nearest neighbor antiferromagnetic arrangement. They found that the A-type arrangement had no stable moments, similar to the ferromagnetic, while the C-type showed a very weak magnetic solution, with moments in the Tc LAPW spheres of 0.44 μ_B and an energy lower than the NSP state by only 0.4 meV / Tc. In contrast a very robust solution was found for the G-type ordering. Therefore, at the LSDA level, $SrTcO_3$ should be described not as a local moment system, but as being closer to the itinerant limit.

In standard oxide magnets there are two energy scales. The first is a scale set by intra-atomic Coulomb repulsions, particularly the Hund's coupling, which drive moment formation. This is typically a high energy scale and leads to stable moments at all solid state temperatures. The second scale controls the ordering temperature, and is that associated with the relative orientation of moments on neighboring sites. This is determined by inter-atomic hopping, as for example in the superexchange mechanism. In perovskites it arises from the hybridization between transition metal d orbitals and oxygen p orbitals. Importantly, the ordering temperature is set by the energy differences between different configurations of the moments, and these differences in turn are related to metal oxygen covalency and details of the bonding topology.

In $SrTcO_3$ the larger extent of the Tc $4d$ orbitals relative to e.g. the $3d$ orbitals of Mn lowers the on-site interactions that underlie moment formation, but strongly increases the amount of covalency as seen in the DOS projections. The result is that the two energy scales become comparable and moment formation and ordering are intertwined. This type of situation is often described as itinerant magnetism. This term should however be used with caution, since the moments are not small, and as a result there is a rearrangement of the DOS not only near E_F but over most of the ~ 3 eV wide t_{2g} manifold.

There are two important differences between $SrMnO_3$ and $SrTcO_3$ that imply high ordering temperature in the Tc compound. First of all, the energy scale is increased because of the greater hybridization and the smaller energy splitting between minority and minority spin orbitals (this

enters in the denominator). Secondly, because the moment formation is intimately connected to the magnetic order, competing states, as exemplified by the C-type pattern are suppressed: with two of the six neighboring Tc flipped the moment is strongly reduced, so that even though four neighbors are oppositely aligned for a net favorable alignment of two neighbors, the energy that might have been gained is lost because the moment collapses. This is related to the physics that leads to high ordering temperatures in low moment itinerant magnets such as Cr and Ni. In any case, these two facts provide a qualitative explanation for the high observed Neel temperature.

Turning to the connection of approximate DFT results with experiment, we note that in the Mott case the insulating state is incorrectly described. The band prediction for $SrTcO_3$ would be that it has a metal-insulator transition associated with magnetic order, i.e. that it becomes conducting above T_N. It is not known at present what happens in $SrTcO_3$ from an experimental point of view. However, the $5d$ analogue, $NaOsO_3$, which shows many features in common with $SrTcO_3$, except that T_N=410 K is lower, is reported to have a metal-insulator transition associated with magnetic ordering [36].

3.5 $SrRuO_3$ and itinerant ferromagnetism

As mentioned, the half-filled t_{2g} band is important for the G-type antiferromagnetism in $SrTcO_3$; with G-type order, one has a majority spin band of bonding character that is filled, and a corresponding minority spin band of antibonding character that is empty. Thus one may expect interesting behavior with doping.

Ru is the element next to Tc in the periodic table. Thus $SrRuO_3$ can be roughly viewed as an electron doped $SrTcO_3$. Like $SrTcO_3$, $SrRuO_3$ has an orthorhombic distorted perovskite structure characterized by octahedral tilts. The ground state is metallic and ferromagnetic, with a total spin moment of $\sim$1.6 μ_B on a per Ru basis (this is distributed between Ru and O, however) and a Curie temperature, T_c=160 K [37–39, 41]. The material is of interest in its own right as a rare example of a $4d$ ferromagnet, and also because many of the related ruthenate phases show very unusual physical behavior, much of it related to magnetism and electron correlations. Notably, the layered perovskite, Sr_2RuO_4, which has the same Ru valence and coordination as ferromagnetic $SrRuO_3$, is an apparently triplet superconductor [42, 43], while Ca_2RuO_4 is a Mott insulator [44]. The bilayer perovskite $Ca_3Ru_2O_7$ is a metamagnetic metal and is ferromagnetic within its bilayers, but with very slight alloying by Ti, becomes a G-type antiferromagnetic Mott insulator [45], again showing borderline behavior in ruthenates.

DFT calculations for $SrRuO_3$ show a clear ferromagnetic instability, with parameters (such as moments) that are in accord with experimental measurements. Also, like $SrTcO_3$, but in contrast to $SrMnO_3$, the moments are highly dependent on the magnetic order; in $SrRuO_3$ the moments are suppressed for G-type order. Also, there is a strong dependence on structure. Without the octahedral tilting, i.e. with the cubic perovskite structure the moment is reduced from 1.59 μ_B per formula unit to 1.17 μ_B in the LSDA [40]. $CaRuO_3$, which differs structurally from the Sr compound in having larger tilts due to the smaller ionic radius of Ca, is paramagnetic although highly enhanced (i.e. very near ferromagnetism) according to experiment. This is in accord with
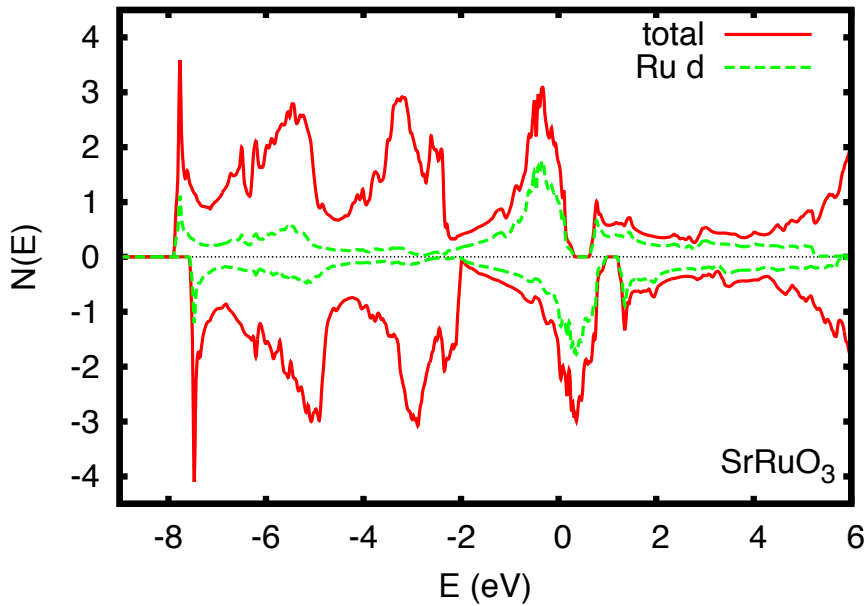
Fig. 6: *Electronic density of states of SrRuO$_3$ as obtained within the LSDA (see Ref. [40]) on a per formula unit basis. The Ru d projections are onto the LAPW spheres of radii 2.0 Bohr.*

LSDA calculations [46], although within the LSDA CaRuO$_3$ is closer to ferromagnetism than in experiment. This may be a sign of renormalization due to quantum spin fluctuations associated with the proximity to the ferromagnetic state. Such renormalizations are not described by standard approximate DFT calculations, because the electron gas upon which these approximations are based is at densities that place the uniform electron gas far from magnetism [47–49]. In any case, the strong dependence of the moments on the ordering as well as on the structure indicate an itinerant aspect to the magnetism.

The interplay between moment formation and magnetic order discussed above for SrTcO$_3$ and SrRuO$_3$ is a characteristic common to many $4d$ and $5d$ magnetic oxides. Essentially, compared to $3d$ magnets, (1) the Coulomb interactions, including the exchange interactions are relatively weaker since they depend on Slater integrals, which are smaller for more extended orbitals and (2) the hopping and covalency involving the d orbitals is stronger, as these larger orbitals overlap more strongly with orbitals on neighboring O atoms. These two characteristics are generic to such materials.

Another aspect that is important is that because of the heavier atoms involved, spin orbit can play a more important role. Although we do not discuss this in detail here, we note that it has received recent attention both in terms of correlation effects in materials such as iridates [50], and in providing mechanisms for high magnetocrystalline anisotropies and magneto-optical coefficients. This may be important from a practical point of view especially in ferromagnetic (or ferrimagnetic) materials with heavy element moments and Curie temperatures above room temperature, such as double perovskites (e.g. Sr$_2$CrReO$_6$ [51]).

Fig. 6 shows the calculated density of states of orthorhombic SrRuO$_3$ in its ferromagnetic

ground state as obtained within the LSDA (this is a new calculation, done similarly to that reported in Ref. [40] but with a better converged zone sampling; the moment of 1.55 μ_B in this calculation is slightly lower than in the reference, 1.59 μ_B). The electronic structure shows exchange split bands that are otherwise similar between the majority and minority spin. The region near the Fermi energy is derived primarily from Ru t_{2g} states as expected. However, even in the π bonding t_{2g} manifold strong hybridization with O is evident. This can be seen clearly in the DOS via the Ru d bonding contributions to the nominal O $2p$ bands.

$SrRuO_3$ provides an example of itinerant magnetism. In its simplest form it arises from an instability of the Fermi surface, but in general the moments are finite and states away from the Fermi surface are important as well. In any case, in the simplest picture, if the density of states at the Fermi energy, $N(E_F)$ is high then a system may lower its energy by an exchange splitting where the majority spin states move to higher binding energy (lower absolute energy) relative to the minority spin and accordingly charge is transferred from the minority to the majority channel as seen in the DOS. This instability is described by Stoner theory [52], and was generalized to the case of finite moments in the so-called extended Stoner theory [53] (ref. [46] discusses ruthenates from this point of view).

Within Stoner theory, the bare Pauli susceptibility ($\chi_0 = N(E_F)$, with suitable units) is enhanced by a factor $(1-N(E_F)I)^{-1}$, where $N(E_F)$ is expressed on a per spin basis. An instability towards ferromagnetism occurs when the Stoner parameter, $N(E_F)I$ exceeds unity. The physical origin of I is in the exchange interaction, i.e. through the Coulomb repulsion, and therefore more compact orbitals lead to larger I, while covalency reduces I. The Stoner criterion amounts to a criterion that the gain in exchange energy from polarizing the bands exceeds the loss in kinetic energy due to the unequal occupation. Typical values of I for $3d$ transition elements are in the range 0.7-0.8 eV, and so a Stoner instability can be anticipated if $N(E_F)$ for a $3d$ transition atom exceeds $\sim 1.3\,\mathrm{eV}^{-1}$ on a per spin per atom basis. Values for various elements can be found in Ref. [54]. However, it should be noted that while these values are useful for understanding the type of magnetic behavior that is expected in a given material, in practice the precise value of I varies from material to material and one would not use the tabulated values of I, but would directly obtain the susceptibility and magnetic behavior from self-consistent calculations.

Actually, the Stoner enhancement, above, is a special case of the RPA enhancement, which can be written,

$$\chi(\mathbf{q}) = \chi_0(\mathbf{q})/(1 - I(\mathbf{q})\chi_0(\mathbf{q})), \qquad (7)$$

where χ_0 is the bare Lindhard susceptibility, and $I(\mathbf{q})$ is an interaction term that is now $\mathbf{q}$-dependent. As in the case of ferromagnetism, an instability occurs when the product $I(\mathbf{q})\chi_0(\mathbf{q})$ reaches unity, in this case towards a spin density wave at the nesting vector, $\mathbf{q}$. Details and interesting discussion about itinerant magnetism from a band structure point of view can be found in the book of Kubler [55].

Returning to $SrRuO_3$, one sees a substantial peak in the DOS, which is what drives the magnetic instability. Because this peak is derived from hybridized bands rather than pure d bands a rigid splitting will result in a magnetization density that reflects this character, i.e. the character of the band states near the Fermi energy. In the case of $SrRuO_3$ this is approximately 2/3 from

Ru t_{2g} states and 1/3 from O $2p$ states (note that there is always ambiguity in defining where contributions to states come from as there is no unique physical decomposition of the charge density into atomic contributions). In SrRuO$_3$ the t_{2g} bands do in fact exchange split rather rigidly as can be seen by comparing the majority and minority DOS, and similarly for the Ru d projection of the DOS. The reason why the bands exchange-split rigidly in this way is that the energy cost associated with breaking the Ru - O hybridization is high in this material. In any case, the consequence is the prediction of substantial moments on the O sites amounting in aggregate to $\sim$1/3 of the total magnetization. This has been confirmed by neutron diffraction measurements.

Another consequence of the induced spin-polarization on O is that not only the $p\pi$ states of O that are hybridized with the polarized Ru t_{2g} orbitals are exchange-split, but as seen in the DOS, the entire O $2p$ manifold is exchange-split. This includes the lower part that comes from the $p\sigma$ orbitals.

As was discussed in Ref. [46], the ferromagnetic ground state of SrRuO$_3$ can be analyzed using extended Stoner theory. Extended Stoner analysis helps shed some additional light on the general features of the magnetic instabilities in ruthenates. The key parameter in this theory is $N(E_F)I$, where the Stoner I is a normally atomic-like quantity giving the local exchange enhancement. Generally, I is determined by the density distribution on an ion, and is larger for more compact orbitals, as in $3d$ ions relative to $4d$ ions. In compounds, I is replaced by a material dependent average I. The appropriate averaging for calculating the energetics is with the decomposed DOS, $I = I_A n_A^2 + I_B n_B^2$, for two components, A and B, where I_A and I_B are the Stoner I for atoms A and B, and n_A and n_B are the fractional weights of A and B in $N(E_F)$ (normalized to $n_A + n_B = 1$). The O^{2-} ion is highly polarizable (it does not exist outside crystals) and because of this the value of I_O may be expected to be material dependent. Nonetheless, O^{2-} is a small ion and so I_O may also be large. Mazin and Singh got I_{Ru}=0.7 eV and $I_O = 1.6$ eV for SrRuO$_3$, yielding $I = 0.38$ eV including O and $I = 0.31$ eV without the O contribution. The O contribution to I is generic to perovskite derived ruthenates, as it simply reflects the hybridization of the t_{2g} orbitals of nominally tetravalent octahedrally coordinated Ru with O. This provides a ferromagnetic interaction between Ru ions connected by a common O. The interaction comes about because for a ferromagnetic arrangement the O polarizes, and this contributes to the energy, while for a strictly antiferromagnetic arrangement, O does not polarize by symmetry, and so in this case there is no O contribution to the magnetic energy. This is local physics and so this contribution to the paramagnetic susceptibility, while peaked at the zone center, is smooth in reciprocal space.

This ferromagnetic tendency, which is generic to all the ruthenates, competes with an antiferromagnetic nesting related tendency in the layered perovskite Sr$_2$RuO$_4$, which is a superconductor. In that compound, spin-fluctuation theory predicts that the ferromagnetic tendency provides an interaction that can stabilize the triplet state [56, 57]. It is not clear what the role of the antiferromagnetic tendency is in the superconductivity, but one possibility is that it competes with the ferromagnetic tendency, moving the system away from magnetic ordering and thus allowing triplet superconductivity to appear as the ground state.

3.6 Summary

There are a wide variety of oxide magnets, including many useful materials. In spite of many decades of productive research on these, entirely new systems and new physics continue to be discovered in oxides. The above represents a narrow selection of three materials that illustrate some concepts (and leaves out other very important topics, e.g. orbital ordering). Nonetheless, I hope that it is useful.

4 Concluding remarks

Life would be much less interesting (and perhaps not existent at all) in a universe where all substances had roughly the same properties, e.g. a world where all solids had the mechanical properties of Jello. Fortunately for us this is not the case, and instead condensed matter displays a richly varied diversity of properties. According to density functional theory, all of this variety is fundamentally associated with the different charge-density distributions in materials. If one considers that the valence charge-density is most important, it is remarkable to observe that the average valence-density in a material like diamond is not so much different from that in iron or $BaTiO_3$ even though the properties of those substances are very different. As mentioned, solids are not like blueberry muffins. From this point of view it is most remarkable that approximate DFT methods, such as the LDA, effectively describe many of these differences even though it would seem at least superficially to be based on a description adapted from the uniform electron gas. This success, which is reflected in the widespread use of approximate DFT in condensed matter physics, chemistry and materials science, often provides a very useful starting point for understanding correlated materials and their properties.

Acknowledgements

References

[1] H. Hohenberg and W. Kohn, Phys. Rev. **136**, B864 (1964)

[2] W. Kohn and L.J. Sham, Phys. Rev. **140**, A1133 (1965)

[3] J.P. Perdew, K. Burke and M. Ernzerhof, Phys. Rev. Lett. **77**, 3865 (1996)

[4] J.P. Perdew, J.A. Chevary, S.H. Vosko, K.A. Jackson, M.R. Pederson, D.J. Singh and C. Fiolhais, Phys. Rev. B **46**, 6671 (1992)

[5] W.E. Pickett, Rev. Mod. Phys. **61**, 433 (1989)

[6] W.E. Pickett, H. Krakauer, R.E. Cohen and D.J. Singh, Science **255**, 54 (1992)

[7] D.J. Singh and M.H. Du, Phys. Rev. Lett. **100**, 237003 (2008)

[8] I.I. Mazin, D.J. Singh, M.D. Johannes and M.H. Du, Phys. Rev. Lett. **101**, 057003 (2008)

[9] R.G. Parr and W. Yang, *Density Functional Theory of Atoms and Molecules* (Oxford Press, New York, 1994)

[10] R.M. Dreizler and J. da Provincia, *Density Functional Methods in Physics* (Plenum, New York, 1985)

[11] M. Ernzerhof, J.P. Perdew and K. Burke, *Density Functionals: Where Do They Come From, Why Do They Work?*, in *Topics in Current Chemistry*, vol. 180, R.F. Nalewajski (ed.) (Springer, Berlin, 1996)

[12] S. Lundqvist and N.H. March, *Theory of the Inhomogeneous Electron Gas* (Plenum, New York, 1983)

[13] J. Callaway and N.H. March, in *Solid State Physics*, H. Ehrenreich and D. Turnbull (eds.), vol. 38, pp. 135 (1984)

[14] D. Ceperley, Nature (London) **397**, 386 (1999)

[15] U. von Barth and L. Hedin, J. Phys. C **5**, 1629 (1972)

[16] L. Nordstrom and D.J. Singh, Phys. Rev. Lett. **76**, 4420 (1996)

[17] D.C. Langreth and M.J. Mehl, Phys. Rev. Lett. **47**, 446 (1981)

[18] J.C. Slater, Phys. Rev. **81**, 385 (1951)

[19] D.J. Singh, Solid State Commun. **98**, 899 (1996)

[20] W.E. Pickett and D.J. Singh, Phys. Rev. Lett. **72**, 3702 (1994)

[21] N.P. Ong, Phys. Rev. B **43**, 193 (1991)

[22] G.H. Jonker and J.H. van Santen, Physica (Amsterdam) **16**, 337 (1950);
G.H. Jonker and J.H. van Santen, Physica (Amsterdam) **16**, 559 (1950)

[23] C. Zener, Phys. Rev. **82**, 403 (1951)

[24] J.B. Goodenough, Phys. Rev. **100**, 564 (1955)

[25] C.W. Searle and S.T. Wang, Can. J. Phys. **48**, 2023 (1970)

[26] R. von Helmolt, J. Wecker, B. Holzapfel, L. Schultz and K. Samwer,
Phys. Rev. Lett. **71**, 2331 (1993)

[27] S. Jin, T.H. Tiefel, M. McCormack, R.A. Fastnacht, R. Ramesh and L.H. Chen,
Science **264**, 413 (1994)

[28] W.E. Pickett and D.J. Singh, Phys. Rev. B **53**, 1146 (1996)

[29] A.A. Belik, Y. Matsushita, T. Katsuya, M. Tanaka, T. Kolodiazhnyi, M. Isobe and
E. Takayama-Muromachi, Phys. Rev B **84**, 094438 (2011)

[30] H. Sakai, S. Ishiwata, D. Okuyama, A. Nakao, H. Nakao, Y. Murakami, Y. Taguchi and
Y. Tokura, Phys. Rev. B **82**, 180409 (2010)

[31] J.A. Souza, J.J. Neumeier, R.K. Bollinger, B. McGuire, C.A.M. dos Santos, and
H. Terashita, Phys. Rev. B **76**, 024407 (2007)

[32] P.W. Anderson, Phys. Rev. **115**, 2 (1959)

[33] J.B. Goodenough, *Magnetism and the Chemical Bond* (Wiley, New York, 1963)

[34] J. Kanamori, J. Phys. Chem. Solids, **10**, 87 (1959)

[35] E.E. Rodriguez, F. Poineau, A. Llobet, B.J. Kennedy, M. Avdeev, G.J. Thorogood,
M.L. Carter, R. Seshadri, D.J. Singh and A.K. Cheetham,
Phys. Rev. Lett. **106**, 067201 (2011)

[36] Y.G. Shi, Y.F. Gao, S. Yu, M. Arai, A.A. Belik, A. Sato, K. Yamaura, E. Takayama-
Muromachi, H.F. Tian, H.X. Yang, J.Q. Li, T. Varga, J.F. Mitchell and S. Okamoto,
Phys. Rev. B **80**, 161104 (2009)

[37] J.J. Randall and R. Ward, J. Am. Chem. Soc. **81**, 2629 (1959)

[38] J.M. Longo, P.M. Raccah and J.B. Goodenough, J. Appl. Phys. **39**, 1327 (1968)

[39] A. Kanbayashi, J. Phys. Soc. Jpn. **44**, 108 (1978)

[40] D.J. Singh, J. Appl. Phys. **79**, 4818 (1996)

[41] G. Cao, S. McCall, M. Shepard, J.E. Crow and R.P. Guertin, Phys. Rev. B **56**, 321 (1997)

[42] Y. Maeno, H. Hashimoto, K. Yoshida, S. Nishizaki, T. Fujita, J.G. Bednorz and
F. Lichtenberg, Nature (London) **372**, 532 (1994)

[43] A.P. MacKenzie and Y. Maeno, Rev. Mod. Phys. **75**, 657 (2003)

[44] S. Nakatsuji and Y. Maeno, Phys. Rev. Lett. **84**, 2666 (2000)

[45] X. Ke, J. Peng, D.J. Singh, T. Hong, W. Tian, C.R. Dela Cruz and Z.Q. Mao,
Phys. Rev. B **84**, 201102 (2011)

[46] I.I. Mazin and D.J. Singh, Phys. Rev. B **56**, 2556 (1997)

[47] T. Moriya and A. Kawabata, J. Phys. Soc. Jpn. **34**, 639 (1973)

[48] M. Shimizu, Rep. Prog. Phys. **44**, 329 (1981)

[49] A. Aguayo, I.I. Mazin and D.J. Singh, Phys. Rev. Lett. **92**, 147201 (2004)

[50] B.J. Kim, H. Ohsumi, T. Komesu, S. Sakai, T. Morita, H. Takagi and T. Arima,
Science **323**, 1329 (2009)

[51] F.D. Czeschka, S. Geprags, M. Opel, S.T.B. Goennenwein and R. Gross,
Appl. Phys. Lett. **95**, 062508 (2009)

[52] E.C. Stoner, Proc. Roy. Soc. London Ser. A **169**, 339 (1939)

[53] G.L. Krasko, Phys. Rev. B **36**, 8565 (1987)

[54] J.F. Janak, Phys. Rev. B **16**, 255 (1977)

[55] J. Kubler, *Theory of Itinerant Electron Magnetism* (Clarendon, Oxford, 2000)

[56] I.I. Mazin and D.J. Singh, Phys. Rev. Lett. **79**, 733 (1997)

[57] I.I. Mazin and D.J. Singh, Phys. Rev. Lett. **82**, 4324 (1999)